Mode-matched phase diffractive optical element for detecting laser modes with spiral phases

Michael A. Golub,[1,*] Liran Shimshi,[2] Nir Davidson,[2] and Asher A. Friesem[2]

[1]Department of Physical Electronics, Faculty of Engineering, Tel Aviv University, Ramat Aviv 69978, Israel
[2]Department of Physics of Complex Systems, Weizmann Institute of Science, Rehovot 76100, Israel

*Corresponding author: mgolub@eng.tau.ac.il

Received 15 March 2007; revised 8 July 2007; accepted 21 September 2007;
posted 4 October 2007 (Doc. ID 81031); published 2 November 2007

A new type of diffractive optical element for detecting and measuring the power distribution of transverse modes emanating from radially symmetric laser resonators is presented. It is based on a relatively simple straightforward design of a phase-only diffractive optical element that serves as a matched filter, which correlates between specific prerecorded transverse modes with a certain azimuthal mode order and those in the incident laser light. Computer simulations supported by experimental results demonstrate how such elements can accurately detect modes with spiral phases and provide quantitative results on the modal power distribution. © 2007 Optical Society of America

OCIS codes: 140.3300, 050.1970, 050.1380.

1. Introduction

It is often advantageous to determine and shape the distributions of modes in the output laser beam and to diagnose whether one mode or a mix of several modes exist [1–7]. Typically, the modal distribution is estimated by visual inspection, but such inspection is inadequate for most applications that involve sensitive optical sensors [8,9], feedback loops in adaptive optics, and diagnostics of temperature induced changes in high power lasers, as well as for laser beam characterization [7,10]. Other far field image processing techniques for extracting modal composition suffer from nonlinearities, have limited dynamic range, and involve complicated time consuming digital processing [11,12]. Still other techniques involve high quality computer generated diffractive optical elements (DOEs), designed by efficient iterative or cell oriented procedures for converting a complex transmittance function into a phase function (encoding) [4,6,7,10,13–17].

In this paper we consider a new type of phase only DOE with which it is possible to simultaneously detect several transverse modes with different azimuthal mode orders and obtain quantitative results on modal power distribution. Such a mode-matched DOE is designed in a relatively simple straightforward procedure for directly obtaining the required phase function, with no need for complicated encoding. It incorporates several multiple carrier spatial frequencies, where, at each spatial frequency, a mode with a certain azimuthal mode order is detected. Quantitative experimental results on modal power distribution are presented.

2. Basic Principles and Optical Correlation Arrangement

In radially symmetric laser cavities and fiber lasers a mixture of either several degenerate Laguerre–Gaussian transverse modes $\mathrm{TEM}_{p,l}$ or nondegenerate Laguerre–Gaussian transverse modes $\mathrm{TEM}_{p,l}^{*}$ exist. These have the form of

$$\psi_{p,l}(r,\ \varphi) = R_{p,l}(r)\cos(l\varphi), \quad \text{degenerate,} \tag{1}$$

$$\psi_{p,l}(r,\ \varphi) = R_{p,l}(r)\exp(il\varphi), \quad \text{nondegenerate,} \tag{2}$$

where r and φ are the polar coordinates, $R_{p,l}(r)$ is a real valued function of the polar radius, $p = 0, 1, 2 \ldots$ is the radial mode order, $l = 0, \pm 1, \pm 2 \ldots$ is the azimuthal mode order, and $l\varphi$ is a spiral phase. The two dimensional orthogonality property

0003-6935/07/327823-06$15.00/0

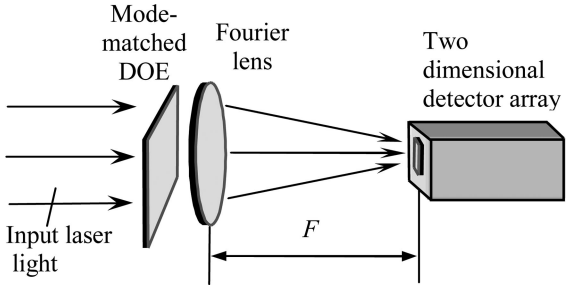

Fig. 1. Basic optical arrangement for mode detection and measurements.

of $\psi_{p,l}(r, \varphi)$ is provided by the orthogonality of $R_{p,l}(r)$ in the radial coordinate r and the orthogonality of $\exp(il\varphi)$ and $\cos(l\varphi)$ in the angular coordinate φ. In order to detect modes with a different azimuthal order l we need to exploit only the orthogonality in the angular coordinate φ. Accordingly, $R_{p,l}(r)$ can simply be replaced by any radial function $R(r)$.

The basic optical arrangement for such mode detection is schematically shown in Fig. 1. It includes the mode-matched DOE, a focusing Fourier lens with a focal length F, and a two dimensional detector array in the focal plane of the lens. The mode-matched DOE contains a set of conjugate spiral phases $-l\varphi$, where l ranges from $-l_{\max}$ to $l_{\max}$, each on a different spatial frequency carrier. With the optical arrangement, correlation peaks are obtained at the detector array when the input light contains the corresponding modes [4]. The correlation peak for each azimuthal mode order l occurs at a different location. The desired complex transmittance function for the mode-matched DOE can be written as

$$T = \sum_l t_l \exp\left[i\left(-l\varphi + 2\pi\nu^{(l)}x\right)\right], \tag{3}$$

where x is a Cartesian coordinate in the DOE plane, $\nu^{(l)}$ is the carrier spatial frequency for azimuthal mode order l, and t_l is the complex weight given to each azimuthal mode order l. Accordingly, the correlation peak for each l occurs at $\lambda F\nu^{(l)}$ along the x coordinate of the detector plane, where λ is the laser wavelength. Separation between different correlation peaks is ensured by resorting to sufficiently large spatial frequencies $\nu^{(l)}$, while the correlation results from the interaction between conjugate spiral phases $-l\varphi$ in T and spiral phases $l\varphi$ of the respective modes in the input laser beam. The modal power distribution can be directly measured as the intensity distribution among the correlation peaks.

It should be noted that the modal phase distribution can also be measured by the recording and processing of microinterferograms in the vicinity of the correlation peaks. Moreover, the size and beam quality M^2 of the incident beam do not affect the correlation results. A differing beam divergence will merely shift the correlation peaks but not affect the relative correlation results.

3. Mode-Matched Diffractive Optical Element

The mode-matched DOE can best be implemented with a phase only transmittance function. We start with the phase φ_c for a component with azimuthal order $l = 1$ in Eq. (3), written as

$$\varphi_c = -\varphi + 2\pi\nu^{(1)}x, \tag{4}$$

where $\nu^{(1)}$ is the carrier spatial frequency for azimuthal mode order $l = 1$. We now introduce a phase nonlinearity [18] $Q(\varphi_c)$ to obtain the phase only transmittance function $\exp[iQ(\varphi_c)]$. Such a phase only transmittance function can be expanded in a Fourier series, to yield

$$\begin{aligned} T = \exp[iQ(\varphi_c)] &= \sum_{l=-\infty}^{\infty} t_l \exp(il\varphi_c) \\ &= \sum_{l=-\infty}^{\infty} t_l \exp\left(-il\varphi + i2\pi l\nu^{(1)}x\right), \end{aligned} \tag{5}$$

where the complex Fourier coefficients t_l are

$$t_l = \frac{1}{2\pi}\int_0^{2\pi} \exp[iQ(\varphi_c) - il\varphi_c]\mathrm{d}\varphi_c. \tag{6}$$

Comparing Eqs. (3) and (5) leads to

$$\nu^{(l)} = l\nu^{(1)}. \tag{7}$$

As is evident from Eq. (7), the carrier spatial frequency for each azimuthal mode order l, i.e., $\nu^{(l)}$, is a multiple of $\nu^{(1)}$ and therefore lies along the same axis as $\nu^{(1)}$. This results from the fact that the transmission function T in Eq. (5) can be represented as a one dimensional Fourier series. It should be noted that the use of the phase nonlinearity $Q(\varphi_c)$ has led directly to a phase only transmittance function without the need to resort to complicated complex-to-phase encoding.

A particular shape of nonlinearity $Q(\varphi_c)$ in Eqs. (5) and (6), which provides weight coefficients t_l that have a constant modulus value $|t_l|$ for $|l| \le l_{\max}$ and zero value for $|l| > l_{\max}$, may be found by the spot array generation method [19–21]. Accordingly, we designed and fabricated a typical mode-matched DOE containing a set of five conjugate spiral phases $l = -2, -1, 0, 1$, and 2 ($l_{\max} = 2$), and using carrier spatial frequency $\nu^{(1)}$. Although the mode-matched DOE can be fabricated with high resolution electron-beam (e-beam) lithography [6,16,17], we resorted to a relatively simpler technology mainly for the purpose of demonstration. For the fabrication we started with a computer generated pattern $Q[-\varphi + 2\pi\nu^{(1)}x]$, which was converted to a gray level mask by relatively simple low resolution photographic slide recording equipment that limited the carrier spatial frequency to $\nu^{(1)} = 5$ lines/mm. The pattern of the gray level mask was then transferred, by means of contact printing, onto a photopolymer medium to form the final phase

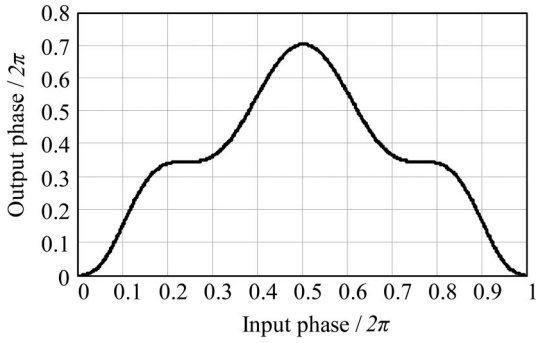

(a)

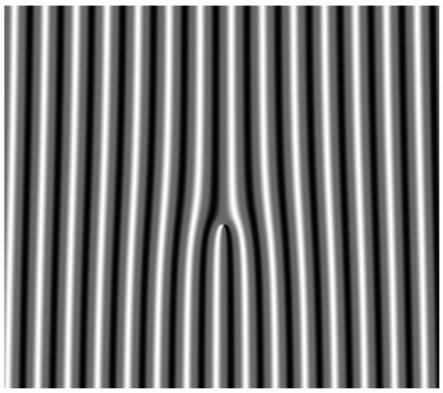

(b)

Fig. 2. Typical mode-matched DOE that has five diffraction orders of equal intensities and a carrier spatial frequency of 5 lines/mm: (a) nonlinearity function $Q(\varphi_c)$ for each groove; and (b) central part of the gray level mask of the desired phase function.

only mode-matched DOE with a diameter of 7 mm. The mode-matched DOE is shown in Fig. 2. Figure 2(a) shows the shape of the phase nonlinearity $Q(\varphi_c)$ that was found by an iterative algorithm, where $Q(\varphi_c)$ essentially defines the phase profile of each groove. Figure 2(b) shows a central part of the gray level mask of the desired phase function.

4. Calculated and Experimental Results

We calculated the correlations among six different input modal distributions and the mode-matched DOE shown in Fig. 2. For the calculations, and subsequently for the experiments, we used a focal length $F = 154$ mm for the Fourier lens and illumination wavelength of 1.06 μm, so that a spatial frequency of $\nu^{(1)} = 5$ lines/mm will separate the correlation at the detector array plane.

Figure 3 shows the calculated far field intensity distribution of the input modes and correlation results. The input modal distributions were $TEM_{0,-2}$*, $TEM_{0,-1}$*, $TEM_{0,0}$, $TEM_{0,1}$*, $TEM_{0,2}$*, and $TEM_{0,1}$ which is essentially comprised of two nondegenerate modes $TEM_{0,1}$* and $TEM_{0,-1}$*. Figures 3(a)–3(f) show far field intensity distributions of the individual input modes. Figures 3(g)–3(l) show the corresponding far field intensity distributions of the correlation result; the ruler at the bottom of each figure indicates loca-

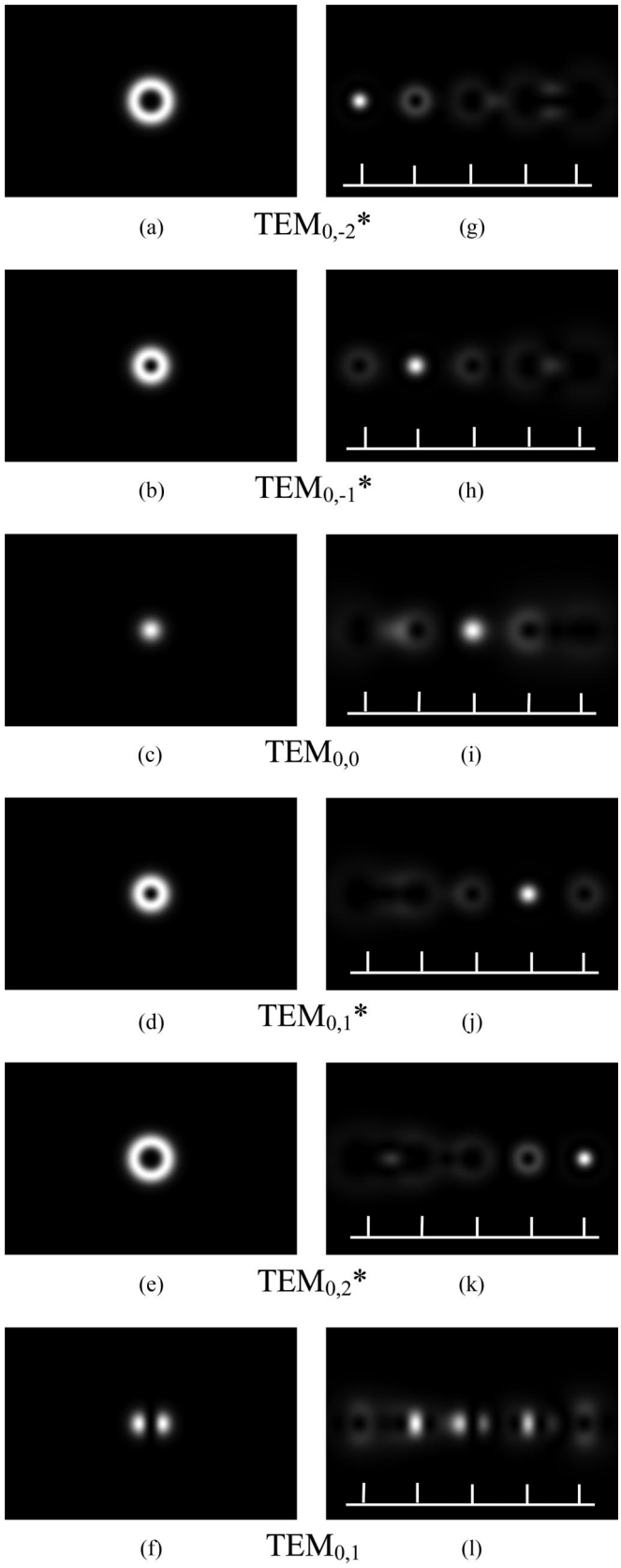

Fig. 3. Calculated far field intensity distributions of the input modes and corresponding correlation results. (a)–(f) Input mode distributions; (g)–(l) correlation results after passing through the mode-matched DOE; white ruler shows expected locations of the correlation peaks according to $\lambda F \nu^{(l)}$.

tions where the correlation peak might occur, according to $\lambda F\nu^{(l)}$. As expected, the mode-matched DOE distributes the light of the input beam into five spatially separated correlation distributions, i.e., autocorrelation and cross correlation. As is evident, Fig. 3(i) shows that, for a $TEM_{0,0}$ Gaussian input, a single correlation peak is obtained at the center of the focal plane. Figures 3(h) and 3(j) show that, for a $TEM_{0,\pm1}$* Laguerre–Gaussian input, a single correlation peak is obtained at the off-axis location of first order diffraction. Figures 3(g) and 3(k) show that, for a $TEM_{0,\pm2}$* Laguerre–Gaussian input, a single correlation peak is obtained at the off-axis location of second order diffraction. Finally, Fig. 3(l) shows the correlation results for a $TEM_{0,1}$ input, which is essentially a superposition of $TEM_{0,1}$* and $TEM_{0,-1}$* inputs with equal powers. Here two symmetrically located correlation peaks are obtained at the proper locations. As is evident, there is also a cross-correlation distribution of two lobes around the zero diffraction order. These lobes are not equal in intensity because of the inherent asymmetry in the spiral phases and carrier spatial frequency orientation in the mode-matched DOE, Eqs. (4) and (5). In general, the results demonstrate that the location of the correlation peaks at the focal plane correspond to the azimuthal mode order. The intensities of the correlation peaks are proportional to the relative intensities of the input modes.

In order to test our mode-matched DOEs, we performed experiments using the arrangement shown in Fig. 1 and the mode-matched DOE shown in Fig. 2. The mode-matched DOE was placed at a distance of 90 mm from the laser output. The Fourier lens of focal length $F = 154$ mm was placed 10 mm from the mode-matched DOE. A CCD camera, located at the focal plane of the Fourier lens, detected the far field intensity distributions of the incident modes as well as the correlation results. Although our mode-matched DOEs can detect the modal distribution of light emerging directly from a laser, in our experiment the different input modal distributions were obtained by letting a nearly Gaussian output beam from a Nd:YAG laser ($\lambda = 1.06$ μm, a beam diameter of 0.9 mm $1/e^2$) pass either through an appropriate continuous spiral phase element [22,23] or a discontinuous binary phase element [24]. Accordingly, the input distributions used in the experiments differ from those $TEM_{0,l}$* modes used in calculations [25,6,26]. Nevertheless, 84% to 93% of the power in the resulting modified complex amplitude distributions represent the desired pure Laguerre–Gaussian transverse modes of $TEM_{0,l}$* [26].

The experimental results are presented in Fig. 4 and Table 1. Figures 4(a)–4(f) show the far field intensity distributions for six input modal distributions along with the elements that were used to form these modes. Figures 4(a)–4(e) show the far field intensity distributions of essentially single nondegenerate modes $TEM_{0,-2}$*, $TEM_{0,-1}$*, $TEM_{0,0}$, $TEM_{0,1}$*, and $TEM_{0,2}$*, and Fig. 4(f) shows the far field intensity distribution of the degenerate $TEM_{0,1}$ mode, which is

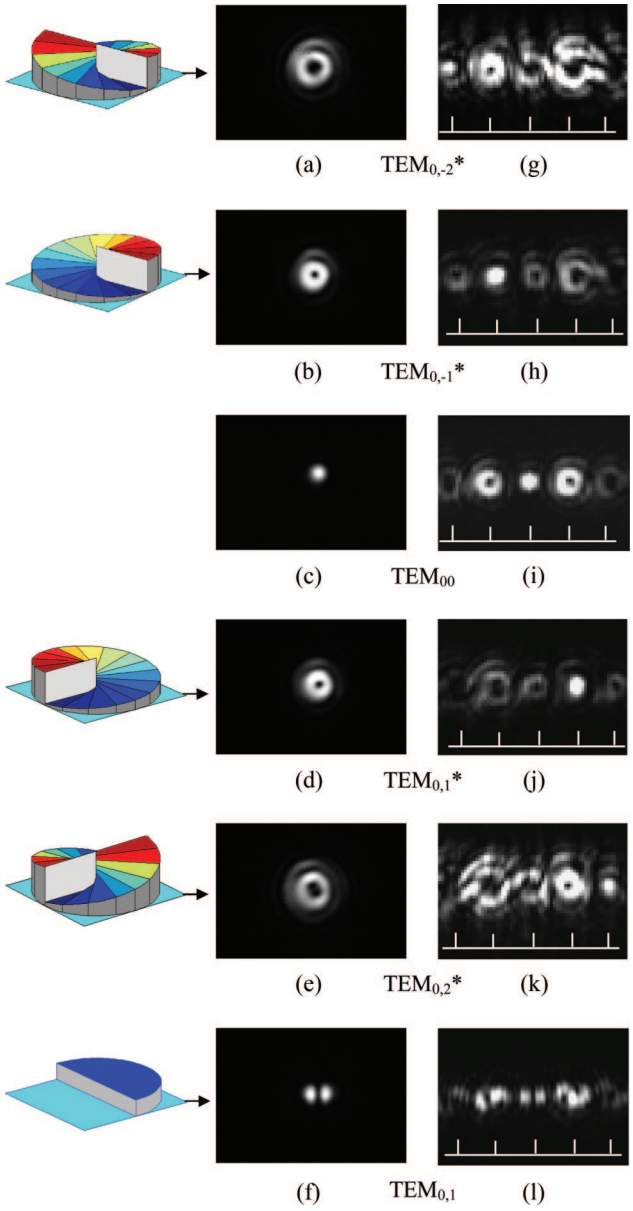

Fig. 4. (Color online) Experimental far field intensity distributions of the input modes and corresponding correlation results. (a)–(f) Input mode distributions along with phase elements for forming these modes as essentially single TEM* or TEM modes, (g)–(l) correlation results after passing through the mode-matched DOE; white ruler shows expected locations of the correlation peaks according to $\lambda F\nu^{(l)}$.

essentially composed of two single nondegenerate modes $TEM_{0,-1}$* and $TEM_{0,1}$*. Figures 4(g)–4(l) show the corresponding correlation results at the output and a ruler pointing to the expected locations of the correlation peaks, according to $\lambda F\nu^{(l)}$. As is evident for each particular essentially single input mode there is a single bright correlation peak at the proper focal plane location, whereas there is a ring and a dark spot at the center of the locations that correspond to the other modes, as depicted in Figs. 4(g)–4(k). When the incident beam has essentially two modes, then the expected two bright correlation

Table 1. Experimental Modal Power Distribution: Normalized Experimental Correlation Intensities at the Output Locations According to $\lambda F v^{(l)}$ for Each of the Six Input Modal Distributions

Output Locations, l	−2	−1	0	1	2
Input Mode					
$TEM_{0,-2}$*	1	0.05	0.01	0.01	0.02
$TEM_{0,-1}$*	0.03	1	0.01	0.01	0.01
TEM_{00}	0.00	0.01	1	0.04	0.00
$TEM_{0,1}$*	0.00	0.01	0.04	1	0.01
$TEM_{0,2}$*	0.00	0.02	0.03	0.03	1
$TEM_{0,1}$	0.02	0.96	0.05	1.00	0.00

Note: The top five rows refer to essentially pure $TEM_{0,l}$* modes, hence a single correlation peak is expected at the column with respective number l. The bottom row refers to the $TEM_{0,1}$ mode, which is an equal superposition of essentially $TEM_{0,-1}$* and $TEM_{0,1}$*, hence two identical correlation peaks are expected in columns number $l = 1$ and $l = -1$.

peaks appear at the locations corresponding to $l = \pm 1$, as depicted in Fig. 4(l).

For a more quantitative characterization, as well as the detection and measurements of modal power distributions, we measured the correlation intensities at each of the output locations, according to $\lambda F v^{(l)}$ with $l = -2, -1, 0, 1$, and 2. The results are summarized in Table 1. In each row we normalized the intensities according to the bright autocorrelation peak intensity for the matched mode. Any intensities that are below 1% are indicated as zero. As expected, the results for inputs with essentially single nondegenerate modes, which are given in the top five rows, contain only one strong correlation peak intensity in each row. In the last row, when the input is of essentially two nondegenerate modes, two strong and nearly identical (with 4% accuracy) correlation peak intensities are obtained as expected. Cross-correlation intensities are much smaller, all below 5% of the strong autocorrelation peak intensity, indicating good signal-to-noise ratio. Therefore our DOE enabled us to present quantitative experimental results on modal power distribution, as compared with the qualitative results of reference [16]. These results indicate that aside from some low cross-correlation intensities there is good agreement with the calculated results at $\lambda F v^{(l)}$ locations in the detector array plane. We attribute the discrepancies mainly to fabrication errors of the DOE, imperfections in the nonlinearity function, and the imperfections in the input modes that lead to the nonuniformity of the power distribution between diffraction orders, some wavefront aberrations, and nonzero cross-correlation intensities.

5. Concluding Remarks

We demonstrated how it is possible to detect and measure the modal power distribution of a laser output by means of a relatively simple computer generated mode-matched phase DOE. Our initial experiments show that the accuracy of mode detections is better than 5%. We expect that these results can be significantly improved by fabricating the mode-matched DOEs with a higher level technology.

References

1. A. A. Ishaaya, N. Davidson, G. Machavariani, E. Hasman, and A. A. Friesem, "Efficient selection of high-order Laguerre–Gaussian modes in a Q-switched Nd:YAG laser," IEEE J. Quantum Electron. **39,** 74–82 (2003).
2. S. Makki and J. Leger, "Mode shaping of a graded-reflectivity-mirror unstable resonator with an intracavity phase element," IEEE J. Quantum Electron. **37,** 80–86 (2001).
3. R. Oron, N. Davidson, A. A. Friesem, E. Hasman, and E. Wolf, "Transverse mode shaping and selection in laser resonators," Prog. Opt. **42,** 325–386 (2001).
4. V. A. Soifer and M. A. Golub, *Laser Beam Mode Selection by Computer Generated Holograms* (CRC Press, 1994).
5. M. A. Golub, A. M. Prokhorov, I. N. Sissakian, and V. A. Soifer, "Synthesis of spatial filters for investigation of the transverse mode composition of coherent radiation," Quantum Electron. **12,** 1208–1209 (1982).
6. S. N. Khonina, V. V. Kotlyar, V. A. Soifer, K. Jefimovs, and J. Turunen, "Generation and selection of laser beams represented by a superposition of two angular harmonics," J. Mod. Opt. **51,** 761–773 (2004).
7. M. R. Duparre, B. Luedge, and S. Schroeter, "Etalons for pure and composite transversal modes," Proc. SPIE **6101,** 61011C (2006).
8. P. R. Herczfeld, M. A. El-Sherif, L. R. Kawase, F. K. Ko, and L. Bobb, "Embedded fiber-optics sensor utilizing the modal power distribution technique," Opt. Lett. **15,** 1242–1244 (1990).
9. M. A. Golub, I. N. Sissakian, V. A. Soifer, and G. V. Uvarov, "Mode-selective fiber sensors operating with computer generated optical elements," Proc. SPIE **1572,** 101–106 (1991).
10. M. R. Duparre, V. S. Pavelyev, V. A. Soifer, and B. Luedge, "Laser beam characterization by means of diffractive optical correlation filters," Proc. SPIE **4095,** 40–48 (2000).
11. K. I. Kitayama, M. Tateda, S. Seikai, and N. Uchida, "Determination of mode power distribution in a parabolic index optical fibers," IEEE J. Quantum Electron. **QE-15,** 1161–1165 (1979).
12. C. M. Warnky, B. L. Anderson, and C. A. Klein, "Determining spatial modes of lasers with spatial coherence measurements," Appl. Opt. **39,** 6109–6117 (2000).
13. H. O. Bartelt, A. W. Lohmann, W. Freude, and G. K. Grau, "Mode analysis of optical fibers using computer-generated matched filters," Electron. Lett. **19,** 247–249 (1983).
14. M. A. Golub, E. L. Kaganov, A. A. Kondorov, V. A. Soifer, and G. V. Uspleniev, "Experimental investigation of a multibeam holographic optical element matched to Gaussian–Laguerre modes," Quantum Electron. **26,** 184–186 (1996).
15. S. N. Khonina, V. V. Kotlyar, R. V. Skidanov, V. A. Soifer, P. Laakonen, and J. Turunen, "Gaussian–Laguerre modes with different indices in prescribed diffraction orders of a diffractive phase element," Opt. Commun. **175,** 301–308 (2000).
16. S. N. Khonina, V. V. Kotlyar, and V. A. Soifer, "An analysis of the angular momentum of a light field in terms of angular harmonics," J. Mod. Opt. **48,** 1543–1557 (2001).
17. A. A. Almazov, S. N. Khonina, and V. V. Kotlyar, "Using phase diffraction optical elements to shape and select laser beams consisting of a superposition of an arbitrary number of angular harmonics," J. Opt. Technol. **72,** 391–399 (2005).
18. M. A. Golub, L. L. Doskolovich, N. L. Kazanskiy, S. I. Kharitonov, and V. A. Soifer, "Computer generated diffractive multifocal lens," J. Mod. Opt. **39,** 1245–1251 (1992).
19. L. L. Doskolovich, V. V. Kotlyar, and V. A. Soifer, "Phase gratings with a prescribed intensity distribution among the diffraction orders," Sov. Tech. Phys. Lett. **17,** 771–772 [P. Zh. Tekh. Fizi. **17,** 54–57 (1991)].
20. R. L. Morrison, "Symmetries that simplify the design of spot array phase gratings," J. Opt. Soc. Am. A **9,** 464–471 (1992).

21. D. Prongue, H. P. Herzig, R. Dandliker, and M. T. Gale, "Optimized kinoform structures for highly efficient fan-out elements," Appl. Opt. **31,** 5706–5711 (1992).
22. S. N. Khonina, V. V. Kotlyar, M. V. Shinkaryev, V. A. Soifer, and G. V. Uspleniev, "The phase rotor filter," J. Mod. Opt. **39,** 1147–1154 (1992).
23. R. Oron, N. Davidson, A. A. Friesem, and E. Hasman, "Continuous phase elements can improve laser beam quality," Opt. Lett. **25,** 939–941 (2000).
24. R. Oron, N. Davidson, A. A. Friesem, and E. Hasman, "Discontinuous phase elements for transverse mode selection in laser resonators," Appl. Phys. Lett. **74,** 1373–1374 (1999).
25. D. Rozas, C. T. Law, and G. A. Swartzlander, Jr., "Propagation dynamics of optical vortices," J. Opt. Soc. Am. B **14,** 3054–3065 (1997).
26. G. Machavariani, N. Davidson, E. Hasman, S. Blit, and A. A. Friesem, "Efficient conversion of Gaussian beam to a high purity helical mode," Opt. Commun. **209,** 265–271 (2002).